The Collapse of Sulfide Columns Within the Axial Seamount in Relation to Thermal and Seismic Activity

Maryka Anderson

University of Washington, Seattle, WA

School of Oceanography, Box 357940

email: maryka@uw.edu

05/25/2018

Abstract

Hydrothermal vents release thermally heated seawater in combination with minerals to form precipitates in the seawater. The precipitates can form small columns that attach to the hydrothermal vents. One example of this occurrence is the hydrothermal vent, Mushroom. This hydrothermal vent is located on Axial Seamount off the coast of Oregon. Within the framework of Axial Seamount, a fiber optic cable network relays data from various sensors to the University of Washington. For the intentions of this study, the sensors documenting temperature and seismic activity were used in conjunction with video documentation. The data was processed over the period of November 2015 to July 2016. We discovered that temperature variations and fluctuations in seismic activity have no direct correlation to the column collapse events. We can conclude that these factors are not extremely relevant to the collapse events and other studies should be done to determine a plausible correlation. A proposal of marine technological advancements, such as a new sensor array to efficiently measure pressure changes, temperature, etc., should be considered to further the advancement of the underwater observatory.

Introduction

Hydrothermal vents are fissures in the ocean crust that release thermally heated seawater generated by interaction with hot crustal rocks (Lilley et al 2003). In the subsea, they are found most commonly near mid-ocean ridges where the ocean crust is spreading apart (Kelley et al 2001). Copious amounts of rising magma cause stress on the oceanic crust and create fracture networks where heated seawater can rise adiabatically to vents on the seafloor. Fluids of sufficiently high temperatures can precipitate iron sulfides, upon mixing with cold, oxygen-rich seawater. These dark colored minerals give the chimneys a black coloring. Not all hydrothermal vent systems have black chimneys. Some have a whiter hue which may be associated with the release of compounds such as silicon, barium and calcium. For this study, the focus was on Axial Seamount. Within the Axial Caldera, a fiber-optic cabled array extends from the seafloor to Pacific City, Oregon. The cable network then transfers real-time data to the University of Washington (figure 1). On the surface of the caldera a network of nodes with sensors monitor the activities of hydrothermal vents and the centralized area of the caldera (figure 2). The area of focus for this study is Ashes vent field, located in the Southwest quadrant of the caldera (figure 2). Specifically, at node MJ0B3 (figure 3) where the hydrothermal vent, Mushroom, (figure 4) has a node with attachments for video footage as well as a thermistor array. These tools will allow us to study of the sulfide columns surrounding Mushroom.

In this doing this, we looked at how thermal and seismic changes play a role in the collapse of the sulfide chimneys at Mushroom. There has not been much research focused on the peculiar behavior of chimneys breaking down after rapid vertical growth, although they are known to be very brittle. Some columns grow only a few centimeters in height while in other instances the columns grow to be meters high. The width of the columns extends over a large range as well. All these changes can occur from the same branch off of the main hydrothermal vent structure and more often than not there are large gaps

in between collapse and regrowth. Despite all these observed changes, few studies have been conducted regarding the reason for these growth and collapse patterns observed in the hydrothermal vent systems in the Caldera. However, the Axial system in general is one of the only sites where there is a long-term study of change following eruptions, documenting microbial communities and the sampling of hydrothermal vent chemistry (Huber et al 2003; Butterfield et al 2004; Opatkeiewicz et al 2009) and Axial Seamount is an ideal location as it is a highly active volcano that sits along the spreading center separating the Juan de Fuca Plate from the Pacific Plate (Delaney and Kelley 2015). Scientists have also documented seismic activity of the seamount from non-cabled sources of data (Dziak and Fox 1999; Bohnenstiehl 2004). While these studies found trends in fluxes and useful observations, none touched on the topic specific to the research surrounding the sulfide columns in this study.

Sulfide columns are a crucial part of the structure of hydrothermal systems in general along the 70,000 km long Mid-Ocean Ridge system, but the growth and collapse of these small sulfide columns though may be very common is still poorly understood. It is prudent to understand these processes as they are an important mechanism by which metal deposits of copper, lead, zinc, gold and silver form in the ocean crust (Dziak and Fox 1999; Bohnenstiehl et al 2004). Understanding how these sulfide deposits grow and evolve can help further our understanding of hydrothermal systems in a larger context and contribute to progress involving more integrated research efforts. This research will also aid geochemists in understanding the magnitude of metalloid production in relation to other oceanographic processes contributing to the overall chemistry of seawater.

Methods

The cabled underwater observatory at Axial Seamount, installed in 2014, allows for continuous transmission of data collected by probes and sensors attached to nodes within the Axial caldera from an active hydrothermal system, known as Ashes Vent Field (Delaney et al 2000; Delaney and Varga 2009;

Delaney and Kelley 2015). The Submarine Optical Cables transfer data from instruments to nodes on a trunk line that extends to the Shore Station in Pacific City, Oregon; Land lines connect the data from the Shore Station to the University of Washington also via the fiber optic cable network (Delaney and Kelley 2015) (figure 1). Within the caldera there are sensors connected to the secondary nodes that collect data from each location of interest (figure 2). In this study data was collected from node MJ03B (figure 3) since it is only two meters away from the hydrothermal vent in question. A seismometer, a thermistor array and a camera are attached to this node.

The camera, installed in 2014, (Delaney and Kelley 2015) provides video footage every three hours at 1.5 Gb/s for a total of 8 clips per day. Through the video clips we could see when the columns collapsed with an error of approximately a nine-hour difference between the presence of a sulfide columns and its descent. The video clips were processed for column collapses by observing the clips from November 2015 through July 2016. The definition of a column collapse was defined as the moment when the sulfide column was no longer in view of the video camera. In many cases, the footage tracked the entire fall of the column. Each time the column met the above criteria, the date and time were recorded. All data from this study was acquired from the OOI website, a public data portal. The seismic and temperature data were used to identify correlations in the sulfide columns collapses found from the video footage over the seven-month period, November 2015 to July 2016. This period was chosen because it is a relatively extensive amount of data, considering how long the observatory has been in place. No eruptions took place during this time-period making the data consistent and removing any errors in the data.

Two seismometers, a thermistor array and a high definition video camera are attached to node MJ03B (figure 2). The seismometers were provided by NSF and the Keck Foundation and placed into the observatory in 2014 (figure 5). The dates of chimney collapses were put into a table where seismic data was organized by date and time. The date and time a column was last seen was in one column and the

date and time of the column collapse was in another column. These time stamps were compared to the data from the seismometer on the days in question to observe if any activity took place when a chimney collapsed.

The thermistor array is a platform that defines temperature variations from a 3-D perspective. It sits a couple meters away from the vent and straddles a fracture in the underlying rock, highlighted by white bacterial mats. The bacterial mats might represent a link to the high temperature Mushroom fluids to the thermistor array, as the vent fluid escapes the seafloor (figure 6). For the purposes of this project only arrays 1 through 7, out of a total 24, were processed for data as they are closest to the seafloor and would give the most accurate readings for the vent fluid. If using arrays 8 through 24, we would encounter tidal issues as well as output from immediate flow which can be hard to factor out from the raw temperature data in this situation. Using the array data, we looked at temperature over time. The date and time of the chimney collapses were then plotted on the array graphs as a singular dot.

Results

From November 2015 to July 2016, 45 collapses were recorded. Through the video clips, (figure 7) we see that the sulfide columns seem to follow three main patterns of growth. One, where they grow quickly but remain relatively short and thin in stature (figure 7a). Two, where they grow slower and are usually thicker in diameter but remain shorter in height (figure 7b) and the third, most usual occurrence, where they grow out of frame (figure 7c). This is usually accompanied by a thicker diameter as well. Overall, the length of time it takes for a column to grow and collapse seems to vary. Some collapse and begin regrowth in less than six hours, others continue to grow for weeks before collapsing and beginning regrowth. Sometimes, as noted in February and April of 2016, they do not develop again for upwards of weeks after a collapse.

The video clips were compared to data from the thermistor array (figure 8). Each red dot on the thermistor lineation represents a moment in time when a collapse event occurred. Spatial grid 1 (figure 8a) had temperatures ranging from 2.5-6 degrees Celsius and the sulfide column collapses occurred at points where temperature was dropping. This was not consistent with every temperature drop. Spatial grid 2 (figure 8b) had temperature ranging from 4-16 degrees Celsius where the collapse events had an inconsistent relationship with the temperature profile. The other spatial grids (figure 8c-8g) had similar profiles to Spatial Grid 2. All showed no correlations to collapse events.

The video logs were also compared to seismic data. No collapse event showed a large spike in the two seismometers nearest Mushroom (table 1). For Seismometer 1 (figure 5), OBSSP1, the one about 1km away from Mushroom, the readings stayed in a magnitude below 1 and some had a negative magnitude. Four collapse dates did not show any seismic event at seismometer 1, December 18th, 2015, December 24th, 2015, January 19th, 2016 and April 29th, 2016. At Seismometer 2 (figure 8), OBSSP2, the one closer to the central area of the caldera, all the measurements stayed below a magnitude of 1. On one of the dates that did not show seismic evidence from seismometer 1, a seismic reading was found at seismometer two. This was for December 18th, 2015. December 24th, 2015, January 19th, 2016 and April 29th, 2016 did not have any seismic readings on seismometer 2. On April 20th, 2016 there was evidence of a seismic event on seismometer 1 but not seismometer 2. For the rest of the seismic events at seismometer 2, the measurements stayed below a magnitude 1 and many were also negative.

Discussion

The possibilities of the mechanism of sulfide column collapse at Mushroom are expansive within the underwater framework of the hydrothermal vent system. It is understood that magma rises from the magma chamber deep below the surface and converts water in the conduits and minerals in the rock into an extremely hot water/mineral solution (figure 9). The heated minerals and water travel up

the larger conduits where they connect to the vent (figure 10) (Lilley et al 2003). The vent continually expels the water and mineral mixture into the cooler ocean water. These minerals combine with the ocean water to form precipitates. This can happen close to vent in the water column or at lesser depths depending on temperature. (Lilley et al 2003). In some instances, a vent has many major conduits for mineral travel. This can lead to large column-like structures within another hydrothermal vent. (Lilley et al 2003). A great example of this is Mushroom. When the mineral Sulfur, from the conduit, mixes with hydrogen in the water column they combine to form sulfide precipitates. On Mushroom, the Sulfide precipitate is made at such an extreme rate the minerals stack on top each other forming a black column on the side of Mushroom (figure 11) which then regularly collapses and regrows.

We developed several hypotheses in hopes of uncovering why the sulfide columns on Mushroom collapsed. One hypothesis we tested was how changes in the temperature gradients affect the column collapse and if it was a direct cause. Changes in temperature can lead to alterations in the crystalline formation of the precipitates and is a well-known cause of precipitate formations in any setting. Another major mechanism tested was seismic activity at Axial. The seismic variations at this plate boundary could lead to column collapse from tremors in the ocean crust. Other possibilities include, the formation of the crystalline sulfide structure itself causing column collapses and changes in the pressure or density gradients. The possibility of changes in the amount of the sulfide precipitates could account for why some stay thin and collapse before they reach one meter in height while others grow for extensive amounts of time prior to collapse. The pressure or density gradients could cause the columns to crack under the intense pressures located at the ocean floor or could compact the sulfide precipitates creating a sturdy form.

Of the four major hypotheses mentioned, one tested in this experiment was the temperature variations. Through assessment of the thermistor array, temperatures closest to Mushroom show no significant correlation between temperature changes at the spatial grids chosen and the time of column

collapses documented from the video logs. Although spatial grid one does appear to show a potential correlation, no other spatial grid shows any sign of correlation. Spatial grid one is closest to the crack in the seafloor expelling hydrothermal fluid. There is potential that this temperature profile would be the most accurate but, we would most likely see this correlation in spatial grid two and possibly three as well. In these two spatial grids no correlation was found therefore the theory is highly unlikely. This conclusion can be drawn from spatial grids four through seven as well. Leaving the impression that this is more of a coincidental pattern at spatial grid one rather than a direct cause of the column collapses.

The other hypothesis tested in this study was a comparison of the seismometer data to the documented collapse times. There seems to be no present correlation between these two factors. The magnitude readings vary widely among collapse dates expelling the idea of a pattern in seismic activity over the time-period. Moments of sulfide column collapse even occurred when the seismometer showed a negative reading. For the seismometer to show a correlation a consistent positive number would need to be present more than 80% of the time. The seismometer readings were not consistent 50% of the time. This leads to the interpretation that seismic activity does not directly affect sulfide columns at Mushroom.

Conclusion

From the data collected, we can conclude that temperature variations and seismic activity surrounding Mushroom are not directly correlated to the collapse of sulfide columns. This leaves the possibility of the other two hypotheses. The crystalline structure hypothesis could be tested by developing a geodesic dome structure encapsulating Mushroom (figure 12). This would allow for the placement of cameras above the hydrothermal vent. In doing this, the cameras could monitor the precipitates at various angles and observe the structural variations inside and outside the sulfide columns. To test the pressure and density gradients an array of pressure and density sensors could be

attached to the geodesic dome and placed directly in the center and outside the columns from above at multiple angles. These sensors would need to be developed and attached to the geodesic dome prior to deployment. The sensors would allow for the collection and comparison of the interior and exterior pressures and densities which would easily expose a large gradient and explain how these gradients act at a hydrothermal vent site. Such insights into the structure and processes of hydrothermal vents might allow conclusions on how the collapse is initiated. Another possibility would be to develop and employ an ROV as part of the submarine observatory to make these measurements and video observations and accompany the sensors in data collection.

The underwater observatory enacted at Axial Seamount proved successful for the parameters of this study. In the short amount of time given, an extensive collection of data was available for use. We could deduct that temperature and seismic events do not have direct correlations to the sulfide column collapse events occurring on Mushroom. More studies should be done of similar methods for the sole purpose of consolidating data and furthering the studies of the environment on Axial Seamount. A greater longitudinal study could produce more compelling evidence of the collapse events. As the observatory grows, more sensors and technology can be introduced. With advancements in marine technology, scientists can conduct larger and more effective studies furthering the scientific community surrounding the hydrothermal vents and other occurrences at Axial Seamount. This allows for other theories to be tested and discussed.

References

Bohnenstiehl, D. R., R. P, Dziak, M. Tolstoy, C. G. Fox, M. Fowler (2004) Temporal and spatial history of the 1999–2000 Endeavour Segment seismic series, Juan de Fuca Ridge. Geochemistry, Geophysics, Geosystems 5, DOI: 10.1029/2004GC000735

Butterfield, D.A., K.K. Roe, M.D. Lilley, J.A. Huber, and J.A. Baross (2004) Mixing, reaction and microbial activity in the sub-seafloor revealed by temporal and spatial variation in diffuse flow vents at Axial Volcano. In The Subseafloor Biosphere at Mid-Ocean Ridges, eds., W.S.D. Wilcock, E.F. DeLong, D.S. Kelley, J.A. Baross, and S.C. Cary, Geophysical Monograph 144, American Geophysical Union, Washington DC., pp. 269-289.

Butterfield, D.A., G.J. Massoth, R.E. McDuff, J.E. Lupton and M.D. Lilley (1990) Geochemistry of hydrothermal fluids from Axial Seamount hydrothermal emissions study vent field, Juan de Fuca Ridge: Subseafloor boiling and subsequent fluid-rock interaction. J. Geophys. Res., 95, 12,895-12,921.

Delaney, J. R., D. S. Kelley. (2015) Next-generation science in the ocean basins: expanding the oceanographer's tool-box utilizing submarine electro-optical sensor networks. Seafloor Observatories, 465-503, DOI: 10.1007/978-3-642-11374-1_18

Delaney, J.R. and R.S. Varga (2009) A 2020 vision for ocean science, In The Fourth Paradigm, Data-Intensive Scientific Discovery. eds., T. Hey, S. Tansley, and K. Tolle, Microsoft Research, pp. 27-38.

Delaney, J.R., G.R. Ross, B. Howe, A.D. Chave, and H. Kirkham (2000) NEPTUNE: Real-time ocean and earth sciences at the scale of a tectonic plate. Oceanography 13, 71-79.

Delaney, J.R., F.N. Spiess, S.C. Solomon, R. Hessler, J.L. Karsten, J.A. Baross, R.T. Holcomb, F. Norton, R.E. Mcduff, F.L. Sayles, J. Whitehead, D. Abbott, and L. Olso (1987) Scientific rationale for establishing long-term ocean bottom observatory/laboratory systems, In Marine Minerals Resource Management Strategies, eds. P.G. Teleki, M.R. Dobson, J.R. Moor, and U. von Stackelber, pp. 389-411.

Dziak, R. P., C. G. Fox (1999) The January 1998 Earthquake swarm at Axial Volcano, Juan de Fuca Ridge: Hydroacoustic evidence of seafloor volcanic activity. Geophysical Research Letters 26, 3429–3432.

Huber, J.A., D.A. Butterfield, and J.A. Baross (2003) Bacterial diversity in a subseafloor habitat following a deep-sea volcanic eruption. FEMS. Micro. Eco., 43, 393-409.

Kelley, D.S., J.A. Karson, D.K. Blackman, G.L. Fruh-Green, D.A. Butterfield, M.D. Lilley, E.J. Olson, M.O. Schrenk, K.K. Roe, G.T. Lebon, and P. Rivizzigno (2001) An off-axis hydrothermal vent field near the Mid-Atlantic Ridge at 30 N., Nature, 412, 415-149. DOI: 10.1038/35084000.

Lilley, M.D., D.A. Butterfield, J.E. Lupton, E.J. Olson (2003) Magmatic events can produce rapid changes in hydrothermal vent chemistry. Nature, 422, 878-881. DOI: 10.1038/nature 01569.

Lupton, J.E., E.T. Baker, and G. Massoth (1999) Helium, heat, and the generation of hydrothermal event plumes at mid-ocean ridges. Earth Planet. Sci. Lett., 171, 343-350.

Figure/Table Captions

Figure 1 – Pictorial of fiber-optic cable network associated with Axial Seamount. Cable goes from Axial Caldera to Pacific City, Oregon. Data is then transmitted to the University of Washington. Provided through novae.ocean.washington.edu.

Figure 2 – Network of cables within the Caldera. The hydrothermal vent of focus is within the Ashes Vent field, found at node MJ03B. Provided through novae.ocean.washington.edu

Figure 3– View of Mushroom hydrothermal vent system with location of probes. Provided by novae.ocean.washington.edu

Figure 4 – Close-up diagram of Mushroom hydrothermal vent. Area of focus in this study can be seen as the arrow labeled 'Iron-sulfide anhydrite chimney venting'.

Figure 5 – Diagram depicting the location of the two short-period seismometers closest to Mushroom. OBSSP1 was defined as 'seismometer 1' and OBSSP2 was defined as 'seismometer 2'.

Figure 6 - Thermistor Array in foreground, Cam and Mushroom in background - white material is made up of fractures in basalt substrate, lined with white bacterial matts known as Beggiotoa a sulfur oxidizing microbe

Figure 7 - This figure depicts ten instances of before and after video images of the sulfide columns. The most left pictures depict an instance when the sulfide column was erect while the right column shows the hydrothermal vent after the sulfide column fell off. The time stamp can be found in the upper right image of each photo. Each row depicts one before and after sequence from the video clips. (a) shows a sulfide column erect on December 2nd, 2015 at a time of 1500. The second clip shows no column on December 2nd, 2015 at 2100. (b) shows a sulfide column on December 20th, 2015 at a time of 0300. The second clip shows no evidence of a column on December 20th, 2015 at 1200. (c) shows column growth on January 30th, 2016 at a time of 0000. The second shot shows no evidence of a column on January 30th, 2016 at 1500. (d) shows column growth on March 27th, 2016 at a time of 0300 and the second clip shows no column on March 28th, 2016 at 0600.

Figure 8 - Graph depicts seawater temperature in degrees Celsius from the thermistor array near Mushroom on the y-axis in comparison to seven-month period, November 2015 to July 2016, shown on the x-axis. Red dots on the graph represent time stamps of when the sulfide columns stopped growing and fell off the hydrothermal vent, Mushroom. Data accessed from the Ocean Observatories Data Portal at oceanobservatories.org, specifically from node MJ03B in the Axial seamount cabled array. (a) Represents spatial grid 1 which is closest to the seafloor, (b) represents spatial grid 2, (c) represents spatial grid 3, (d) represents spatial grid 4, (e) represents spatial grid 5, (f) represents spatial grid 6, and (g) represents spatial grid 7, the array farthest away from the seafloor.

Figure 9 – Representation of mechanisms involved in hydrothermal vent systems. Magma from the magma chamber enters the conduits where is mixes with water and minerals. Another conduit not connected to a vent allows for a release of pressure in the conduits acting on the vent. The water and mineral mixture rises adiabatically up the vent and is released in the water column where is mixes with ocean water creating precipitates and depositing minerals into the water column.

Figure 10 – Diagram showing one main hydrothermal vent with conduit system. Red arrows indicate thermally heated water. Blue arrows indicate cold, ocean water. Arrows with gradient indicate mixing of thermally heated water with cold, ocean water.

Figure 11 – Diagram showing sulfide precipitate column structure where vent fluid is also exiting. . Red arrows indicate thermally heated water. Blue arrows indicate cold, ocean water. Arrows with gradient indicate mixing of thermally heated water with cold, ocean water.

Figure 12 – Diagram depicting geodesic dome method of collecting data for future studies. Cameras and sensors are attached as shown. More sensors at various angles could be attached prior to deployment.

Table 1 - this table shows seismic measurements from two seismometers on the Axial caldera as well as the time and date prior to and after a column collapse. Seismometer 1 (OSSP1) can be found 1 km away from Mushroom attached to node MJ03B while seismometer 2 (OSSP2) can be found in the central caldera node, MJ03F.

Figures/Tables

Figure 1

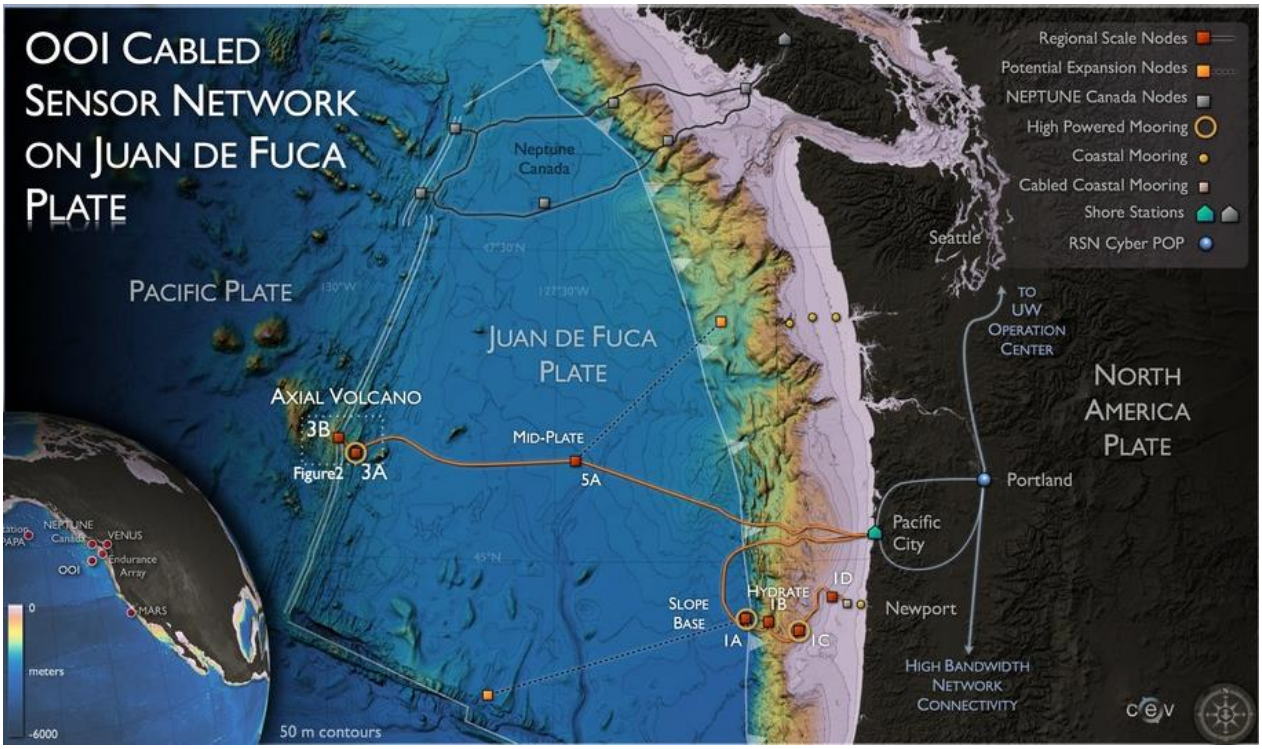

Figure 2

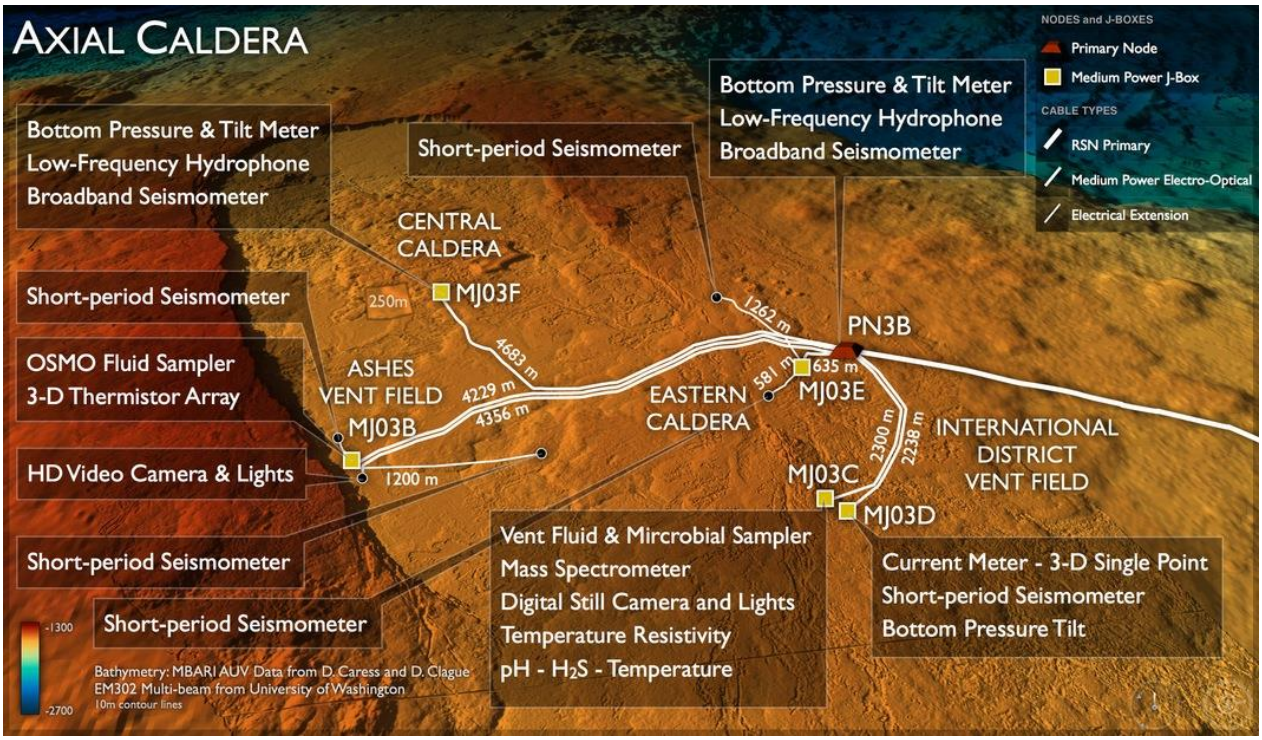
AXIAL CALDERA
NODES and J-BOXES
Primary Node
Medium Power J-Box
CABLE TYPES
RSN Primary
Medium Power Electro-Optical
Electrical Extension
Bottom Pressure & Tilt Meter
Low-Frequency Hydrophone
Broadband Seismometer
Short-period Seismometer
Bottom Pressure & Tilt Meter
Low-Frequency Hydrophone
Broadband Seismometer
CENTRAL CALDERA
Short-period Seismometer
250m
MJ03F
1262 m
PN3B
OSMO Fluid Sampler
3-D Thermistor Array
ASHES VENT FIELD
4683 m
4229 m
4356 m
581 m
635 m
MJ03E
EASTERN CALDERA
MJ03B
2300 m
2238 m
INTERNATIONAL DISTRICT VENT FIELD
HD Video Camera & Lights
1200 m
MJ03C
MJ03D
Vent Fluid & Mircrobial Sampler
Mass Spectrometer
Digital Still Camera and Lights
Temperature Resistivity
pH - H2S - Temperature
Current Meter - 3-D Single Point
Short-period Seismometer
Bottom Pressure Tilt
Short-period Seismometer
-1300
-2700
Bathymetry: MBARI AUV Data from D. Caress and D. Clague
EM302 Multi-beam from University of Washington
10m contour lines

Figure 3

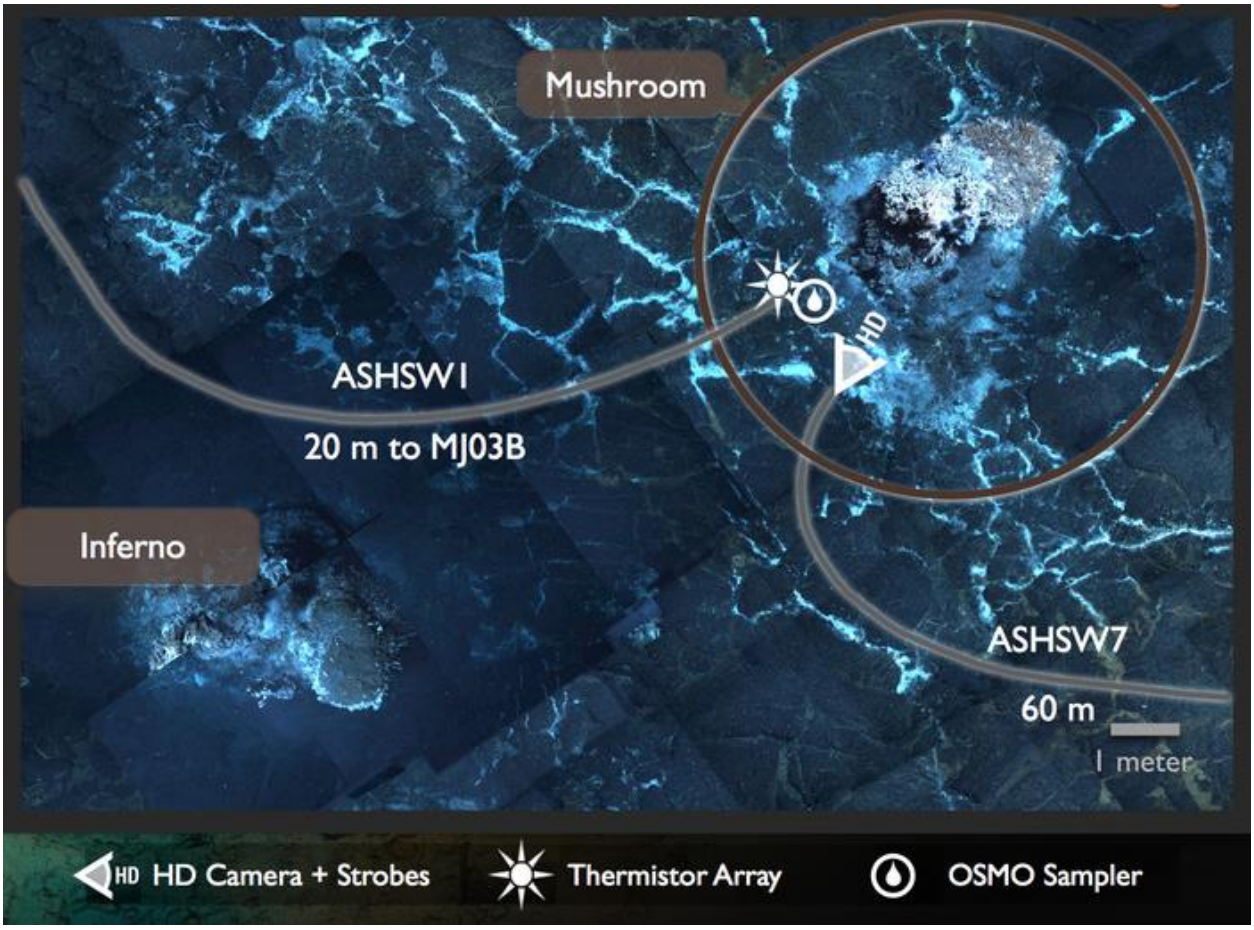
Mushroom
HD
ASHSW1
20 m to MJ03B
Inferno
ASHSW7
60 m
1 meter
HD HD Camera + Strobes
Thermistor Array
OSMO Sampler

Figure 4

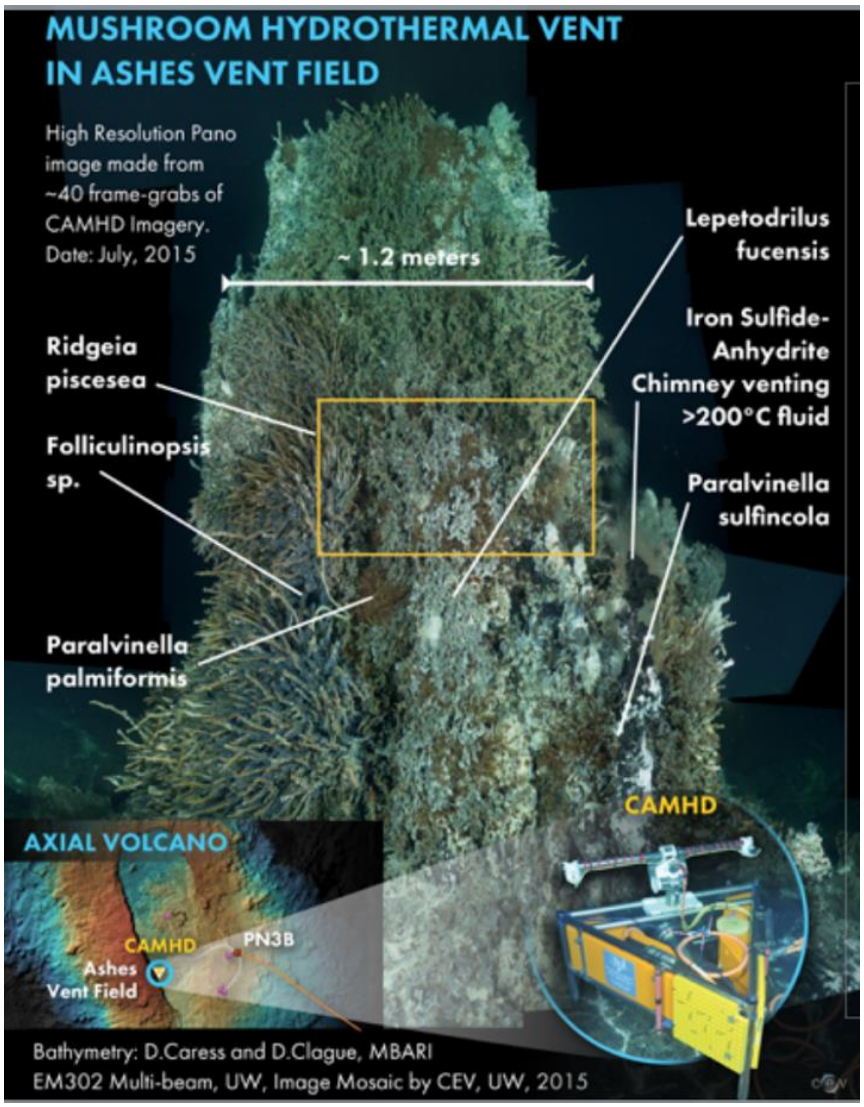
MUSHROOM HYDROTHERMAL VENT
IN ASHES VENT FIELD
High Resolution Pano image made from ~40 frame-grabs of CAMHD Imagery. Date: July, 2015
~ 1.2 meters
Lepetodrilus fucensis
Iron Sulfide-Anhydrite Chimney venting >200°C fluid
Ridgeia piscesea
Folliculinopsis sp.
Paralvinella sulfincola
Paralvinella palmiformis
CAMHD
AXIAL VOLCANO
CAMHD
Ashes Vent Field
PN3B
Bathymetry: D.Caress and D.Clague, MBARI
EM302 Multi-beam, UW, Image Mosaic by CEV, UW, 2015

Figure 5

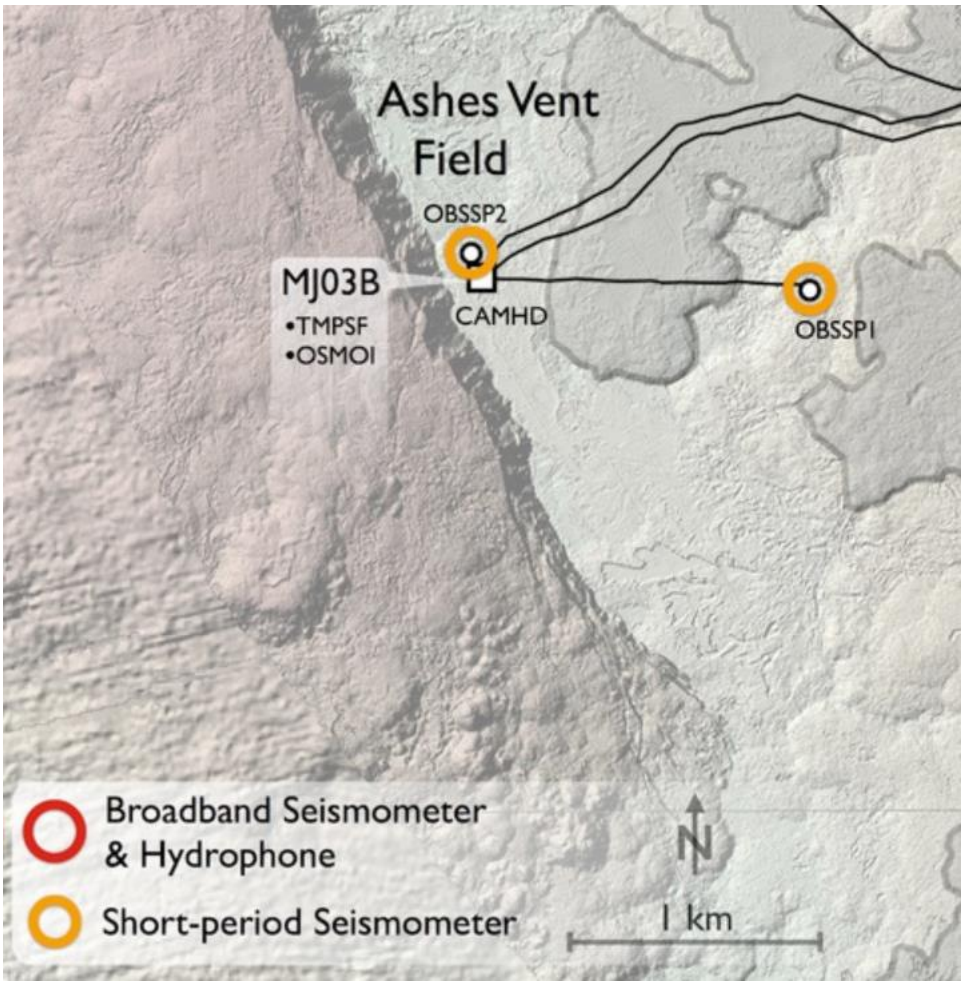
Ashes Vent Field
OBSSP2
MJ03B
•TMPSF
•OSMOI
CAMHD
OBSSP1
Broadband Seismometer & Hydrophone
Short-period Seismometer
N
1 km

Figure 6

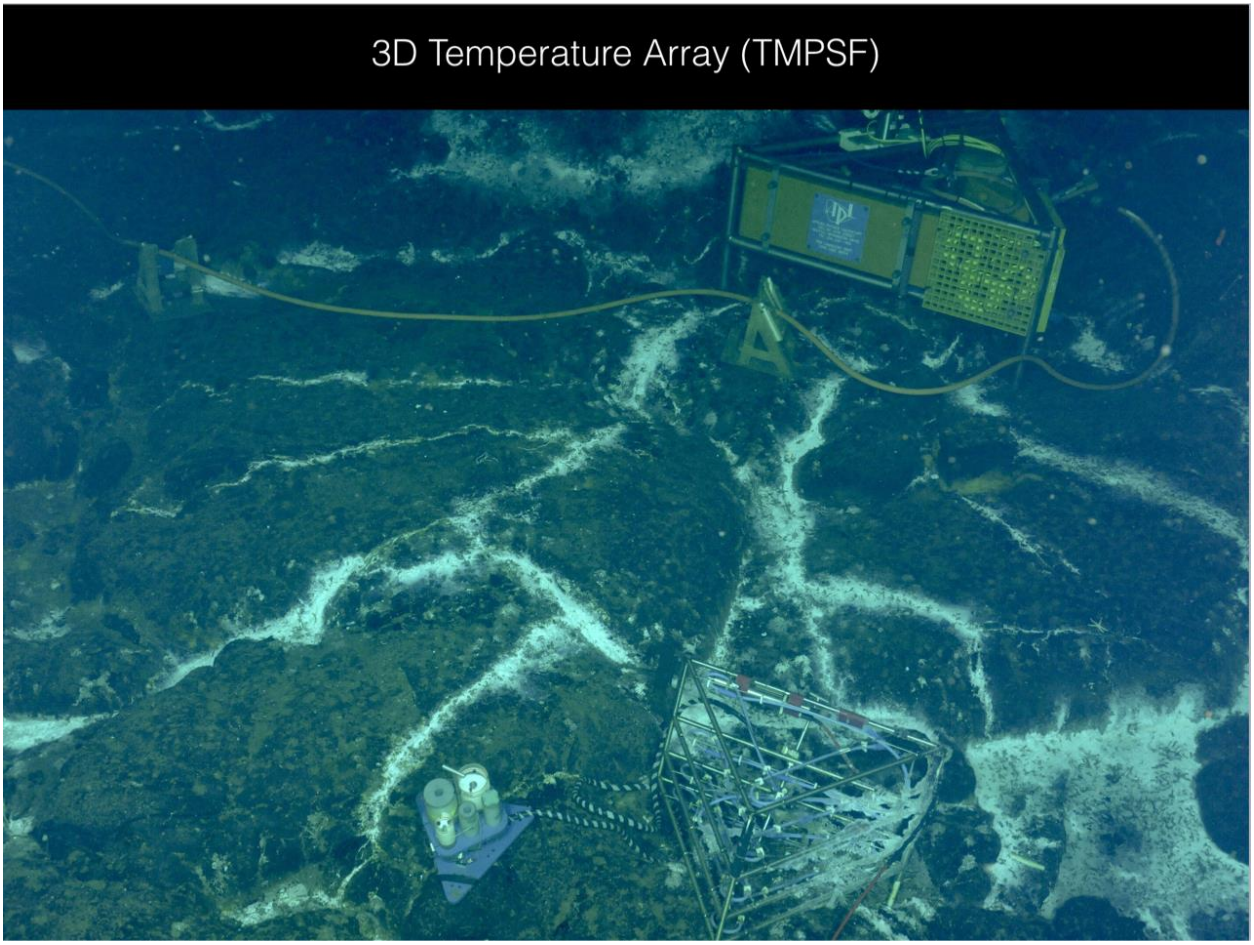

Figure 7

a.

b.

c.

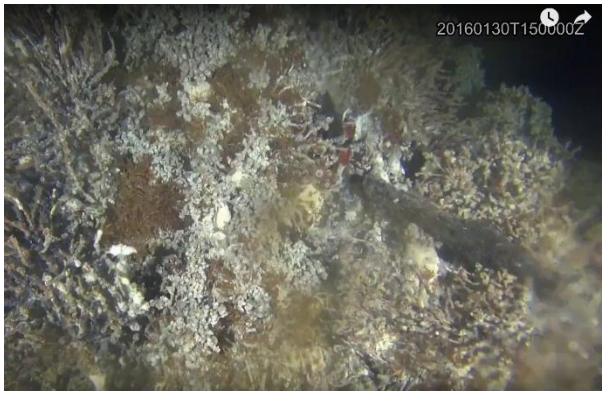

d.

Figure 8

a

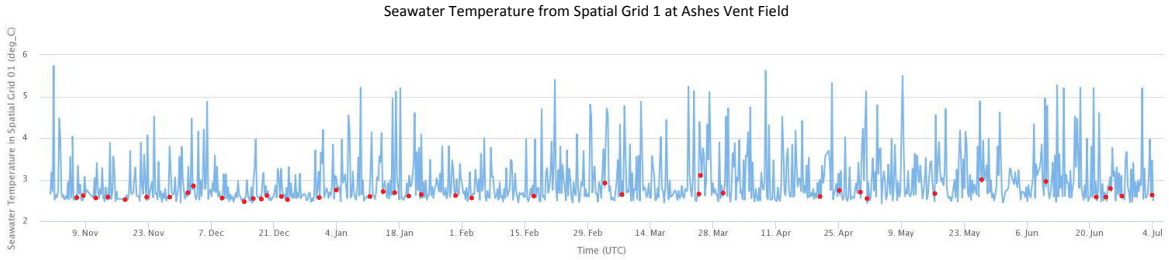

b

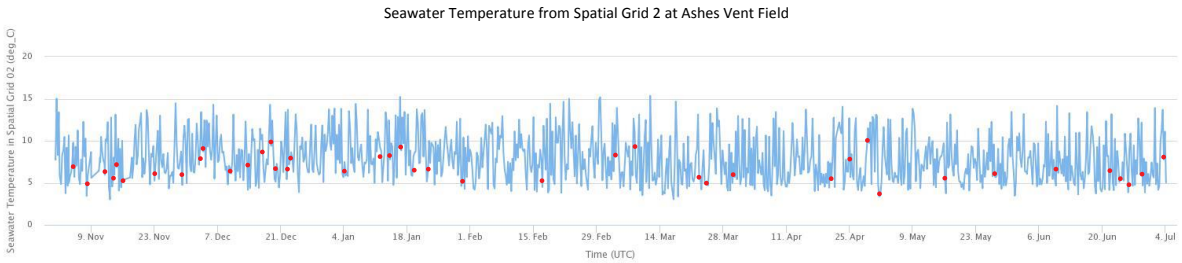

c

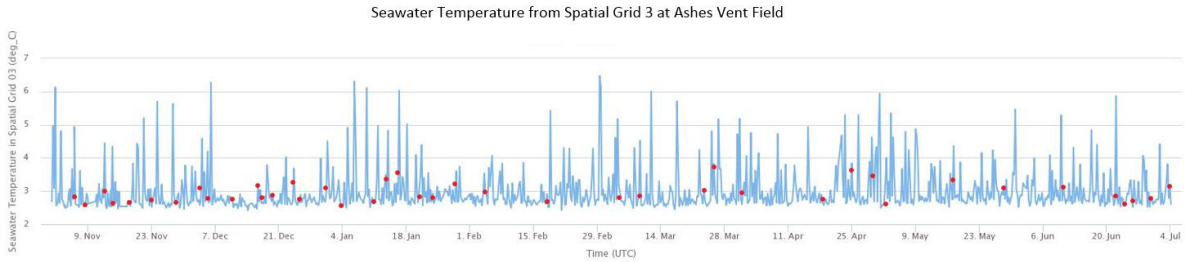

d

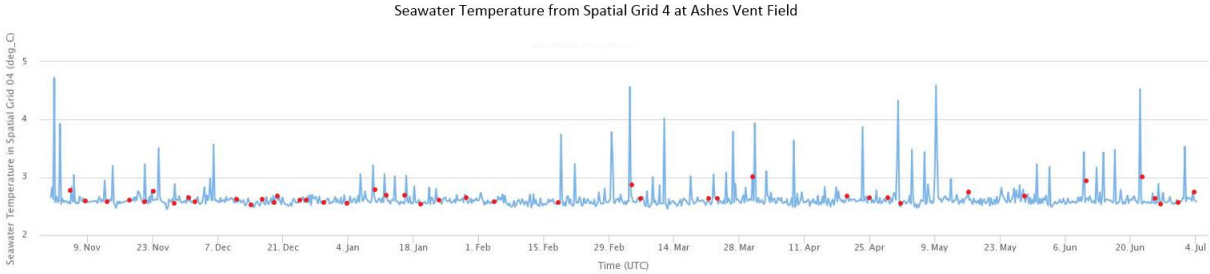

e

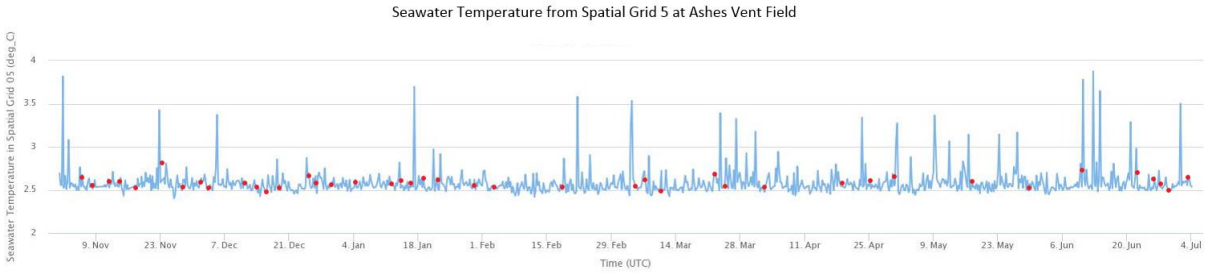
Seawater Temperature from Spatial Grid 5 at Ashes Vent Field
Seawater Temperature in Spatial Grid 05 (deg_C)
4
3.5
3
2.5
2
9. Nov
23. Nov
7. Dec
21. Dec
4. Jan
18. Jan
1. Feb
15. Feb
29. Feb
14. Mar
28. Mar
11. Apr
25. Apr
9. May
23. May
6. Jun
20. Jun
4. Jul
Time (UTC)

f

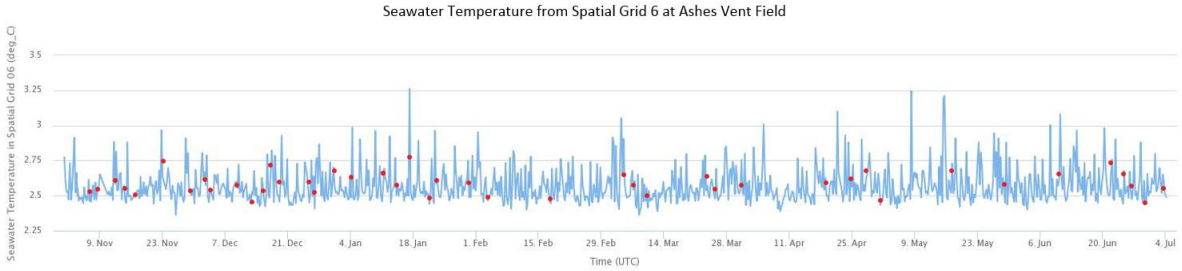
Seawater Temperature from Spatial Grid 6 at Ashes Vent Field
Seawater Temperature in Spatial Grid 06 (deg_C)
3.5
3.25
3
2.75
2.5
2.25
9. Nov
23. Nov
7. Dec
21. Dec
4. Jan
18. Jan
1. Feb
15. Feb
29. Feb
14. Mar
28. Mar
11. Apr
25. Apr
9. May
23. May
6. Jun
20. Jun
4. Jul
Time (UTC)

g

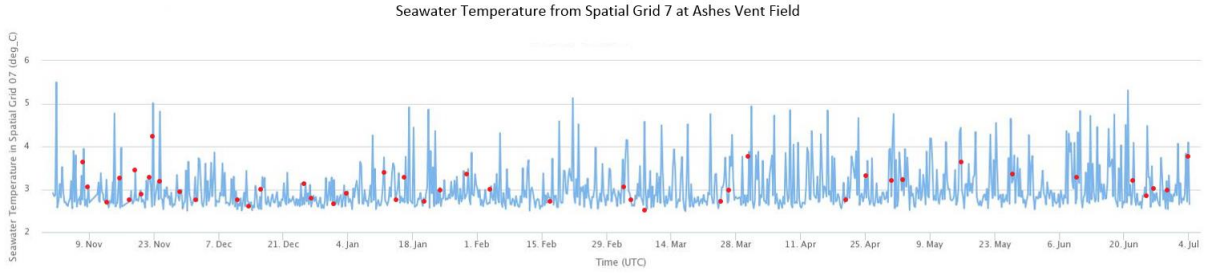
Seawater Temperature from Spatial Grid 7 at Ashes Vent Field
Seawater Temperature in Spatial Grid 07 (deg_C)
6
5
4
3
2
9. Nov
23. Nov
7. Dec
21. Dec
4. Jan
18. Jan
1. Feb
15. Feb
29. Feb
14. Mar
28. Mar
11. Apr
25. Apr
9. May
23. May
6. Jun
20. Jun
4. Jul
Time (UTC)

Figure 9

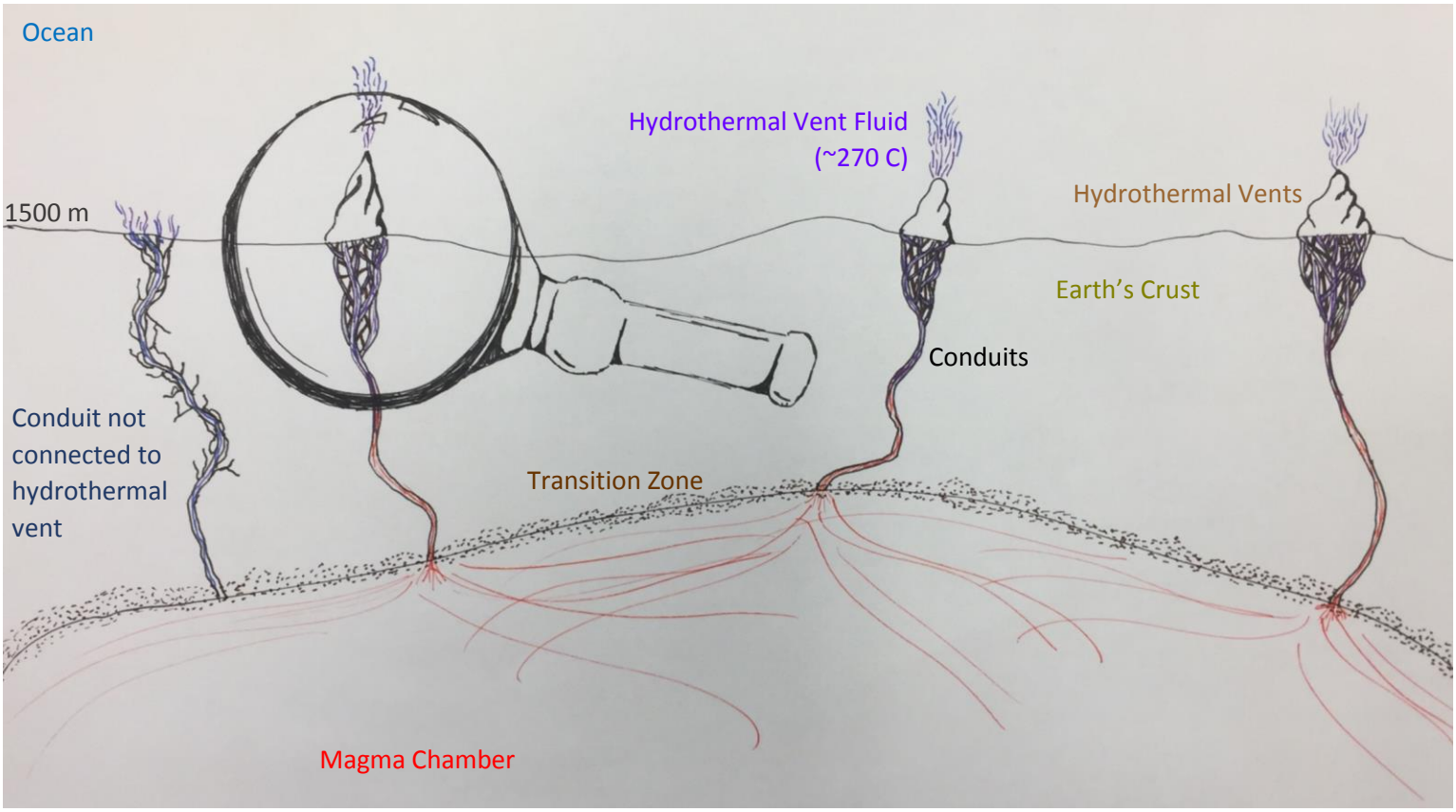
Ocean
Hydrothermal Vent Fluid
(~270 C)
Hydrothermal Vents
1500 m
Earth's Crust
Conduits
Conduit not
connected to
hydrothermal
vent
Transition Zone
Magma Chamber
0
1
2
3
4m
1:100

Figure 10

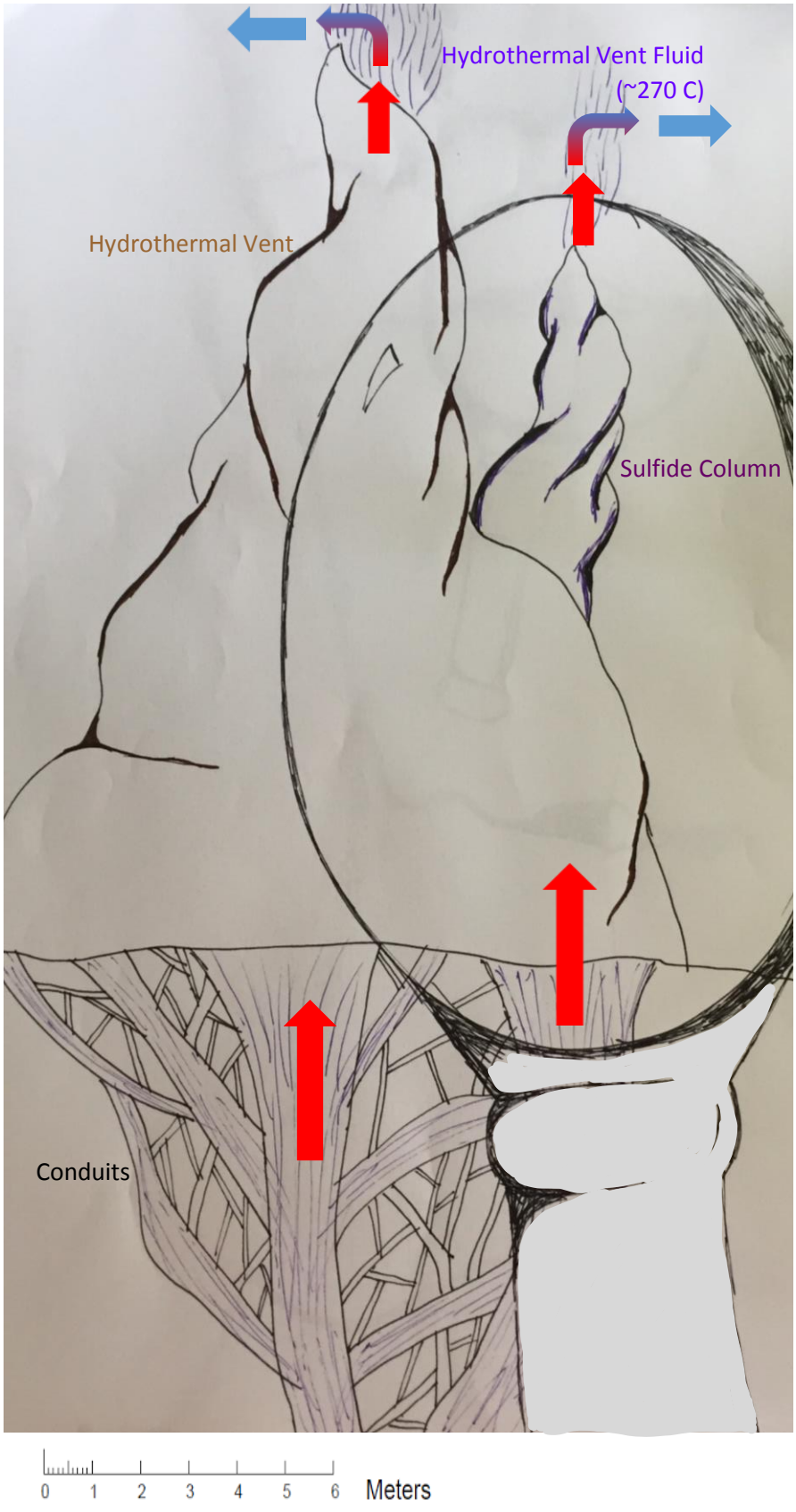
Hydrothermal Vent Fluid
(~270 C)
Hydrothermal Vent
Sulfide Column
Conduits
0 1 2 3 4 5 6
Meters

Figure 11

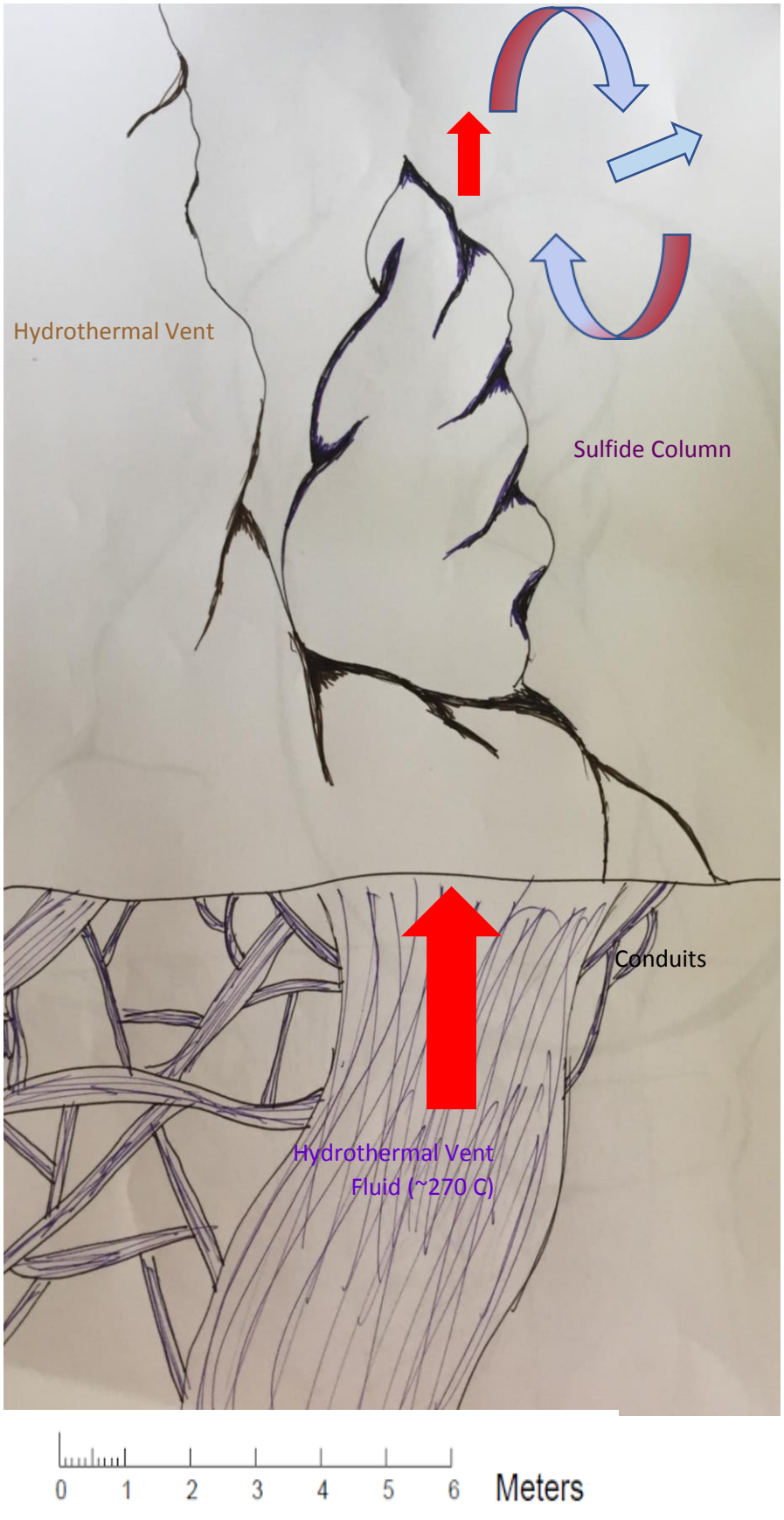
Hydrothermal Vent
Sulfide Column
Conduits
Hydrothermal Vent
Fluid (~270 C)
0
1
2
3
4
5
6
Meters

Figure 12

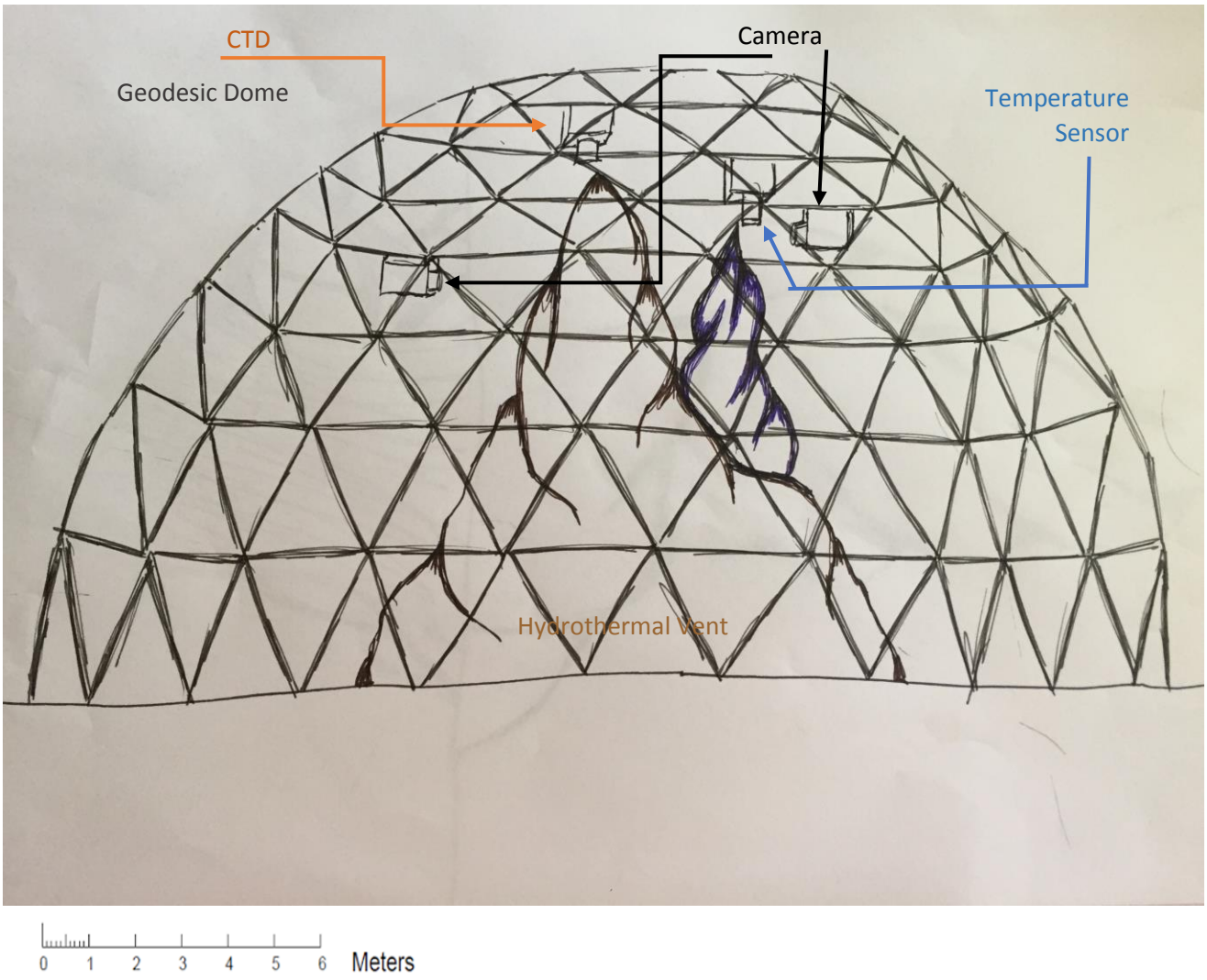
CTD
Geodesic Dome
Camera
Temperature
Sensor
Hydrothermal Vent
0 1 2 3 4 5 6
Meters

Table 1

Date of Collapse Event	Time Column was Last Seen on Video Logs	Inferred Collapse Time	Seismometer 1 (Mw)	Seismometer 2 (Mw)
11/08/2015	1500	2100	0.06	-0.05
11/9/2015	0600	1500	0.27	0.21
11/11/2015	0900	1200	0.09	-0.02
11/13/2015	0900	1200	0.28	0.15
11/16/2015	0900	1200	0.30	0.65
11/23/2015	1200	1500	0.65	0.70
11/28/2015	2100	0000	0.83	0.30
12/02/2015	1500	2100	0.04	0.02
12/04/2015	2100	0000	0.06	0.12
12/09/2015	0000	0300	0.29	0.06
12/13/2015	0600	0900	0.10	0.03
12/16/2015	0000	0300	-0.08	0.02
12/18/2015	1200	1500	*	-0.03
12/20/2015	0300	1200	-0.07	0.04
12/22/2015	0300	1500	0.35	0.50
12/24/2015	1200	1500	*	*
01/01/2016	0300	0600	-0.08	-0.10
01/04/2016	0600	0900	0.46	0.20
01/11/2016	0000	1200	0.38	0.15
01/15/2016	0000	0300	0.01	0.12
01/17/2016	1200	1500	-0.18	0.05
01/19/2016	0300	0600	*	*
01/22/2016	0000	0300	0.15	0.32
01/30/2016	0000	1500	-0.02	-0.10
02/02/2016	0000	0300	-0.20	-0.07
02/15/2016	0000	0300	0.08	-0.02
02/16/2016	0600	0900	0.04	0.01
02/21/2016	0300	1200	-0.10	0.03
03/04/2016	1500	2100	-0.11	-0.08
03/08/2016	1800	2100	-0.15	-0.35
03/24/2016	0300	0600	-0.11	0.03
03/25/2016	0300	0600	0.66	0.44
03/27/2016	0300	0600	0.57	0.23
04/20/2016	1800	2100	-0.24	*
04/25/2016	0600	0900	-0.07	-0.15
04/29/2016	1800	2100	*	*
05/01/2016	0000	0300	0.05	0.23
05/18/2016	0000	1500	0.39	0.41

05/28/2016	1800	2100	0.44	0.06
06/10/2016	0000	0300	0.08	-0.02
06/20/2016	0600	2100	0.42	0.19
06/23/2016	0900	1200	-0.52	-0.24
06/24/2016	1800	2100	-0.11	-0.02